
Enhancing End-to-End Autonomous Driving with Latent World Model

Yingyan Li^{1,2} Lue Fan^{1,2} Jiawei He^{1,2} Yuqi Wang^{1,2} Yuntao Chen³

Zhaoxiang Zhang^{1,2,3✉} Tieniu Tan^{1,2}

¹ Institute of Automation, Chinese Academy of Sciences

² University of Chinese Academy of Sciences

³ CAIR, HKISI, CAS

Email: liyingyan2021@ia.ac.cn

Code: <https://github.com/BraveGroup/LAW>

Abstract

End-to-end autonomous driving has garnered widespread attention. Current end-to-end approaches largely rely on the supervision from perception tasks such as detection, tracking, and map segmentation to aid in learning scene representations. However, these methods require extensive annotations, hindering the data scalability. To address this challenge, we propose a novel self-supervised method to enhance end-to-end driving without the need for costly labels. Specifically, our framework **LAW** uses a LATent World model to predict future latent features based on the predicted ego actions and the latent feature of the current frame. The predicted latent features are supervised by the actually observed features in the future. This supervision jointly optimizes the latent feature learning and action prediction, which greatly enhances the driving performance. As a result, our approach achieves state-of-the-art performance in both open-loop and closed-loop benchmarks without costly annotations.

1 Introduction

End-to-end autonomous driving [15, 22, 30, 40, 14] is increasingly recognized for its potential advantages over traditional methods. The traditional planners cannot access the original sensor data. This leads to information loss and error accumulation [15, 22]. In contrast, end-to-end planners process sensor data to directly output planning decisions, which is shown as a promising area for further exploration.

Most end-to-end autonomous driving methods [15, 22, 14, 30], though operating in an end-to-end fashion, leverage a variety of auxiliary tasks such as detection, tracking, and map segmentation. These auxiliary tasks help the model learn better scene representations. However, they require a large amount of manual annotations, which is quite expensive and limits the data scalability. In contrast, a few end-to-end methods [35, 4, 40] do not adopt perception tasks and only learn from recorded driving videos and trajectories. These approaches can leverage a large amount of available data, making it a promising direction. However, using only limited guidance from trajectories makes it difficult for the network to learn effective scene representations and achieve optimal driving performance.

To address this issue, we enhance end-to-end driving through self-supervised learning, as illustrated in Fig. 1. Traditional self-supervised methods [10, 6] in imaging typically concentrate on static, single-frame images. However, autonomous driving involves a dynamic series of inputs, making it

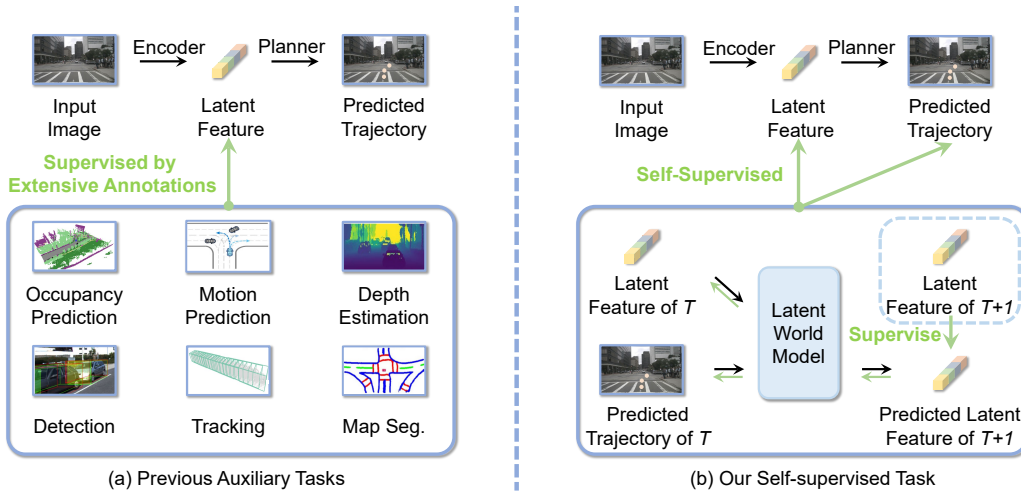


Figure 1: **The comparison between the previous auxiliary tasks and our latent prediction task.** While previous works in (a) rely on auxiliary perception tasks with extensive annotations, we aim to enhance the end-to-end driving model through the latent world model in (b). During training, we obtain the latent feature from the future frame to jointly supervise the latent feature and predicted trajectory of the current frame. Seg.: Segmentation.

essential to use temporal data effectively. A key skill in driving is predicting future conditions based on the current surroundings. Inspired by this, we propose a self-supervised task aimed at forecasting latent features. Specifically, a latent world model is developed to forecast future states based on the current states and ego actions, where the states are represented as the latent scene features within the network. During training, we extract the latent feature of the future frame to supervise the predicted latent feature from the latent world model. As a result, we jointly optimize the latent feature learning and trajectory prediction of the current frame.

Moreover, we establish a simple yet strong planner to extract view-wise latent features and serve as the testbed of the proposed latent world model. Unlike previous methods, this planner does not incorporate ad-hoc modules and perception-related branches, making it more straightforward to understand the inner workings of the latent world model. Given this planner and the latent world model, we have side products. Since the latent world model is capable of predicting future view latent features, we can skip the feature extraction process of some views in the future frame and use the predicted futures of these views as a substitution. By skipping the feature extraction for certain views, we enhance the efficiency of the entire pipeline. To determine which views should be substituted, we propose a view selection strategy. Combined with view latent substitution, this strategy significantly speeds up the whole pipeline with minimal performance loss.

In summary, our main contributions are as follows:

- We propose a **LA**tent **W**orld model for self-supervised learning that enhances the training of end-to-end autonomous driving framework.
- Based on the latent world model, we further propose a view selection strategy, which greatly accelerates the pipeline while incurring minimal performance loss.
- Our framework **LAW** achieves state-of-the-art results on both open-loop and closed-loop benchmarks without manual annotations.

2 Related Works

2.1 End-to-End Autonomous Driving

We divide end-to-end autonomous driving methods [15, 22, 31, 35] into two categories, explicit methods and implicit methods, depending on whether performing traditional perception tasks.

Explicit end-to-end methods [2, 30, 19, 34] perform multiple perception tasks simultaneously, such as detection [24, 17], tracking [45, 37], map segmentation [15, 22] and occupancy prediction [38, 18]. As a pioneering work, P3 [32] employs a differentiable semantic occupancy representation as a cost factor in the motion planning process. Following this, ST-P3 [14] introduces a spatial-temporal feature learning approach to generate more representative features for perception, prediction, and planning tasks concurrently. Then, many works [15, 30, 20, 19] focus on performing detection and BEV map segmentation tasks based on the BEV feature map. As a representative, UniAD [15] integrates multiple modules, including tracking and motion prediction, to support goal-driven planning. VAD [22] explores vectorized scene representation for planning purposes.

Implicit end-to-end methods [35, 4, 43, 40] present a promising direction as they avoid utilizing a large number of perception annotations. Early implicit end-to-end methods [43, 35] primarily relied on reinforcement learning. For instance, MaRLn [35] designed a reinforcement learning algorithm based on implicit affordances, while LBC [4] trained a reinforcement learning expert using privileged (ground-truth perception) information. Using trajectory data generated by the reinforcement learning expert, TCP [40] combined a trajectory waypoint branch with a direct control branch, achieving good performance. However, implicit end-to-end methods often suffer from inadequate scene representation capabilities. Our work aims to address this issue through latent prediction.

2.2 World Model in Autonomous Driving

Existing world models in autonomous driving can be categorized into two types: image-based world models and occupancy-based world models. Image-based world models [11, 39, 12] aim to enrich the autonomous driving dataset through generative approaches. GAIA-1 [12] is a generative world model that utilizes video, text, and action inputs to create realistic driving scenarios. MILE [11] produces urban driving videos by leveraging 3D geometry as an inductive bias. Drive-WM [39] utilizes a diffusion model to predict future images and plans based on these predicted images. Copilot4D [42] tokenizes sensor observations with VQVAE [36] and then predicts the future via discrete diffusion. Another category involves occupancy-based world models [44, 29]. OccWorld [44] and DriveWorld [29] use the world model to predict the occupancy, which requires occupancy annotations. On the contrary, our proposed latent world model requires no manual annotations.

3 Preliminary

End-to-End Autonomous Driving In the task of end-to-end autonomous driving, the objective is to estimate the future trajectory of the ego vehicle in the form of waypoints. Formally, let $\mathbf{I}_t = \{\mathbf{I}_t^1, \mathbf{I}_t^2, \dots, \mathbf{I}_t^N\}$ be the set of N surrounding multi-view images captured at time step t . We expect the model to predict a sequence of waypoints $\mathbf{W}_t = \{\mathbf{w}_t^1, \mathbf{w}_t^2, \dots, \mathbf{w}_t^M\}$, where each waypoint $\mathbf{w}_t^i = (x_t^i, y_t^i)$ represents the predicted BEV position of the ego vehicle at time step $t + i$. M represents the number of future positions of the ego vehicle that the model aims to predict.

World Model In autonomous driving tasks, a world model aims to predict future states based on the current state and actions. To be specific, let $\hat{\mathbf{F}}_t$ represent the features extracted from the current frame at time step t , $\mathbf{W}_t = \{\mathbf{w}_t^1, \mathbf{w}_t^2, \dots, \mathbf{w}_t^M\}$ denote the sequence of planned waypoints by the planner, the world model predicts features $\hat{\mathbf{F}}_{t+1}$ of the future frame using $\hat{\mathbf{F}}_t$ and \mathbf{W}_t .

4 Method

The overall methodology is divided into three parts. First, we develop a strong and general end-to-end planner in Sec. 4.1 to extract latent¹. Next, based on the end-to-end planner, we introduce a world model to predict latent in Sec. 4.2. Finally, the predicted latents can substitute for some unimportant latents so we propose a view selection approach in Sec. 4.3.

4.1 End-to-End Planner with Latent Extraction

To extract effective latent feature, we introduce a general and strong end-to-end planner. Initially, N -view images are processed through an image backbone to extract their respective feature repre-

¹The terms "latent" and "latent feature" convey the same meaning.

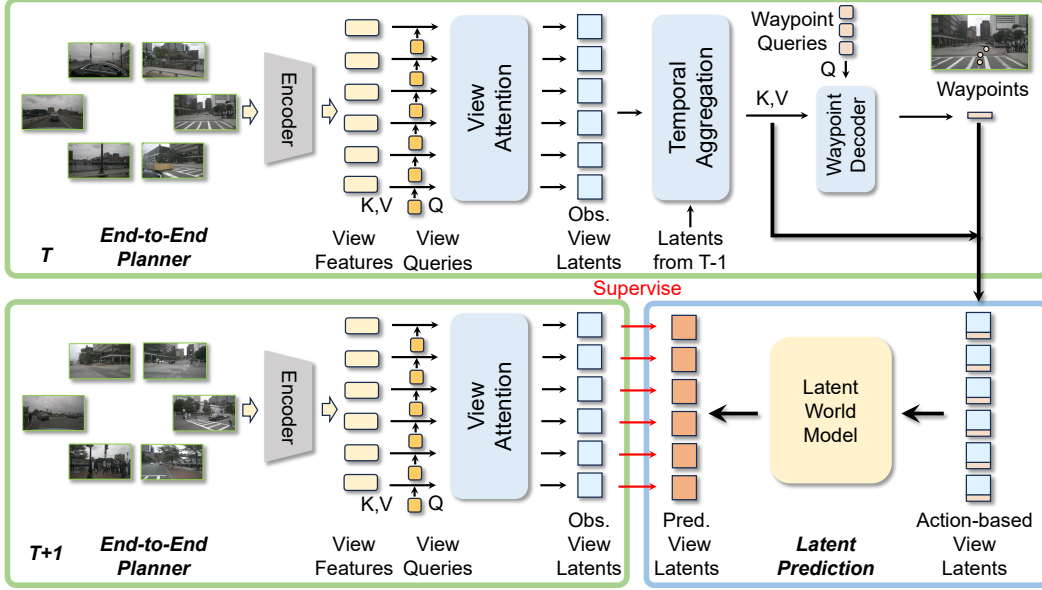


Figure 2: **The overall framework.** Initially, we develop an end-to-end driving framework to extract view latents and predict waypoints. Then, we predict the view latents of the next frame via the latent world model. The predicted view latent is supervised by the observed view latent of the next frame. Obs.: Observed, Pred.: Predicted.

sentations. Following PETR [25], we generate 3D position embeddings for these image features. These position embeddings are integrated with the image features to uniquely identify each view. The enriched image features are denoted as $\mathbf{F} = \{\mathbf{f}^1, \mathbf{f}^2, \dots, \mathbf{f}^N\}$.

Then, we employ a view attention mechanism to compress \mathbf{F} into observed view latent \mathbf{V} . Here, we use the term "observed" to distinguish this view latent from others discussed later in the paper. To be specific, for N views, there are N learnable view queries $\mathbf{Q}_{view} = \{\mathbf{q}_{view}^1, \mathbf{q}_{view}^2, \dots, \mathbf{q}_{view}^N\}$. Each view query \mathbf{q}_{view}^i undergoes a cross-attention with its corresponding image feature \mathbf{f}^i , resulting in N observed view latent $\mathbf{V} = \{\mathbf{v}^1, \mathbf{v}^2, \dots, \mathbf{v}^N\}$, where

$$\mathbf{v}^i = \text{CrossAttention}(\mathbf{q}_{view}^i, \mathbf{f}^i, \mathbf{f}^i). \quad (1)$$

\mathbf{f}^i serves as the key and value of the cross attention. Next, we perform the temporal aggregation to the observed view latent. The observed view latent \mathbf{V} is enhanced by a historical view latent \mathbf{H} , which is generated from the previous frame (the details will be discussed in Sec. 4.2). In this way, we have

$$\mathbf{E} = \mathbf{V} + \mathbf{H}, \quad (2)$$

where \mathbf{E} is named enhanced view latent. Given \mathbf{E} , we develop a waypoint decoder to decode waypoints. This module uses waypoint queries to extract relevant information from \mathbf{E} . To be specific, we initialize M waypoint queries, $\mathbf{Q}_{wp} = \{\mathbf{q}_{wp}^1, \mathbf{q}_{wp}^2, \dots, \mathbf{q}_{wp}^M\}$, where each query is a learnable embedding. These waypoint queries interact with \mathbf{E} through a cross-attention mechanism. The updated waypoint queries are then passed through an MLP head to output the waypoints $\mathbf{W} = \{\mathbf{w}^1, \mathbf{w}^2, \dots, \mathbf{w}^M\}$, which is formulated as:

$$\mathbf{w}^j = \text{MLP}(\text{CrossAttention}(\mathbf{q}_{wp}^j, \mathbf{E}, \mathbf{E})). \quad (3)$$

During training, we use the L1 loss to measure the discrepancy between the predicted waypoints and the ground truth waypoints as:

$$\mathcal{L}_{\text{waypoint}} = \sum_{j=1}^M \|\mathbf{w}_t^j - \mathbf{w}_t^{j, \text{GT}}\|_1, \quad (4)$$

The proposed end-to-end planner extracts the latent simply and effectively, which serves as a good testbed of the latent world model.

4.2 World Model for Latent Prediction

In this section, we utilize the latent world model to predict the view latents of the future frame. To begin with, we generate action-based view latents based on the enhanced view latents \mathbf{E}_t and predicted waypoints \mathbf{W}_t . Specifically, let $\mathbf{E}_t = \{\mathbf{e}_t^1, \mathbf{e}_t^2, \dots, \mathbf{e}_t^N\}$, we convert $\mathbf{W}_t = \{\mathbf{w}_t^1, \mathbf{w}_t^2, \dots, \mathbf{w}_t^M\}$ into a one-dimensional vector $\tilde{\mathbf{w}}_t \in \mathbb{R}^{2M}$. We then concatenate \mathbf{e}_t^i and $\tilde{\mathbf{w}}_t$ along the feature channel dimension. The concatenated vector is transformed by an MLP to form \mathbf{a}_t^i , which matches the feature channel dimension of \mathbf{e}_t^i . Formally, the action-based view latent of the i -th view is denoted as:

$$\mathbf{a}_t^i = \text{MLP}([\mathbf{e}_t^i, \tilde{\mathbf{w}}_t]), \quad (5)$$

where $[\cdot, \cdot]$ denotes the concatenating operation. The overall action-based view latent is $\mathbf{A}_t = \{\mathbf{a}_t^1, \mathbf{a}_t^2, \dots, \mathbf{a}_t^N\}$. Subsequently, given \mathbf{A}_t , we obtain the predicted view latent \mathbf{P}_{t+1} of the frame $t + 1$ by the latent world model:

$$\mathbf{P}_{t+1} = \text{LatentWorldModel}(\mathbf{A}_t). \quad (6)$$

The network architecture of the latent world model is a transformer decoder, which consists of two blocks. Each block contains a self-attention and FFN module. The self-attention is performed in the view dimension. During training, we use the end-to-end planner to extract the observed view latent \mathbf{V}_{t+1} of frame $t + 1$. \mathbf{V}_{t+1} serves as the supervision of \mathbf{P}_{t+1} using an L2 loss function:

$$\mathcal{L}_{\text{latent}} = \sum_{i=1}^N \|\mathbf{p}_{t+1}^i - \mathbf{v}_{t+1}^i\|_2, \quad (7)$$

where $\mathbf{P}_{t+1} = \{\mathbf{p}_{t+1}^1, \dots, \mathbf{p}_{t+1}^N\}$ and $\mathbf{V}_{t+1} = \{\mathbf{v}_{t+1}^1, \dots, \mathbf{v}_{t+1}^N\}$.

Besides, given \mathbf{A}_t , we encode the temporal information into the history view latent \mathbf{H}_{t+1} . \mathbf{H}_{t+1} is used to enhance the observed view latent \mathbf{V}_{t+1} through Eq. (2). To be specific, we conduct self-attention on \mathbf{A}_t in the view dimension, obtaining

$$\mathbf{H}_{t+1} = \text{SelfAttention}(\mathbf{A}_t). \quad (8)$$

\mathbf{H}_{t+1} and \mathbf{P}_{t+1} serve distinct functions. \mathbf{H}_{t+1} aims to encode temporal information as a residual, whereas \mathbf{P}_{t+1} is designed to predict the view latent of the future frame. In addition, \mathbf{P}_{t+1} serves as a good substitute for the observed view latent of future frames, which inspires us to propose the concept of view selection with latent substitution.

4.3 View Selection via Latent Substitution

We propose a view selection approach thanks to the effective view latent predicted by the world model. Taking multi-view videos as input, this approach dynamically selects some informative views to extract features. The other views are not processed and their corresponding view latents are substituted by the predicted view latent from the world model. As shown in Fig. 3, this section consists of three components. First, given several potential view selection strategies, the Selection Reward Prediction component predicts the rewards of these strategies and chooses the strategy with the highest reward. Then, the Planner with Selected Views predicts the trajectory given the selected views. During training, we propose a Selection Reward Labeling module, which assigns a reward label to each selection strategy.

Selection Reward Prediction As illustrated in Fig. 3(a) and (b), we introduce a reward prediction module designed to estimate the reward associated with each selection strategy. The reward quantitatively reflects the effectiveness of the planning outcomes obtained using each strategy. In detail, we define K selection queries. These K selection queries correspond to K potential selection strategies. Each selection query is a learnable embedding. Each strategy selects specific views for processing while discarding the rest. Then, we update the selection queries by performing cross-attention between the queries and the view latent \mathbf{P}_{t+1} predicted by the world model. The updated selection queries are fed into an MLP head to predict the rewards. Given these rewards, we choose the strategy with the highest predicted reward. The strategy is chosen at the frame t and the views selected by this strategy serve as the input of the Planner with Selected Views at frame $t + 1$.

Planner with Selected Views This planner takes selected views as input to produce waypoints as Fig. 3(c) shows. It shares the same weights as the planner in Sec. 4.1. To be specific, Let N represent

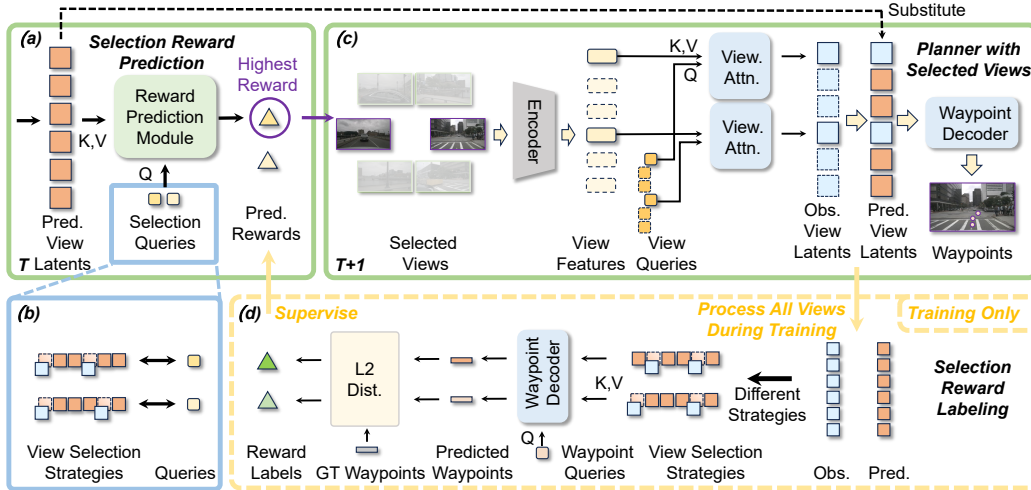


Figure 3: **The pipeline of end-to-end driving with view selection.** Given the predicted view latents, (a) predict rewards for the selection queries defined in (b), where each query corresponds to a selection strategy. Then, we adopt the selection strategy with the best rewards to select views, which serves as the input of the planner in (c). During training, we propose a selection reward labeling module in (d) to label each selection strategy. Pred.: Predicted, Obs.: Observed. L2 Dist.: L2 Distance.

the total number of views. Define $S \subseteq \{1, 2, \dots, N\}$ as the set of indices for views that are selected. \bar{S} is denoted as the complement of S . Given $\mathbf{v}_i \in \mathbf{E}_{t+1}$ and $\hat{\mathbf{v}}_j \in \mathbf{P}_{t+1}$, the combined view latents $\mathbf{v}_{combined}$ are formulated as:

$$\mathbf{v}_{combined} = \bigoplus_{i \in S} \mathbf{v}_i \oplus \bigoplus_{j \in \bar{S}} \hat{\mathbf{v}}_j, \quad (9)$$

where \bigoplus denotes the concatenation operation over the latents in the view dimension. Then, the combined view latents are passed through the same pipeline in Sec. 4.1 to predict trajectories. Based on the Planner with Selected Views, we propose a selection reward labeling module to label the selection strategies.

Selection Reward Labeling We introduce the reward labeling approach as Fig 3(d) shows. Specifically, for the k -th strategy, the corresponding selected views are fed into the Planner with Selected Views to predict waypoints $\hat{\mathbf{w}}_k$. The reward label \hat{d}_k of k -th strategy is defined as the L2 distance between the predicted waypoints $\hat{\mathbf{w}}_k$ and the ground truth waypoints $\hat{\mathbf{w}}^{GT}$ as:

$$\hat{d}_k = -\|\hat{\mathbf{w}}_k - \hat{\mathbf{w}}^{GT}\|_2. \quad (10)$$

The larger \hat{d}_k is, the closer $\hat{\mathbf{w}}_k$ are to the ground truth waypoints $\hat{\mathbf{w}}^{GT}$. During training, we use the L1 loss to learn the rewards, formulated as $\mathcal{L}_{reward} = \sum_{k=1}^K \|d_k - \hat{d}_k\|_1$,

In summary, the total loss of our framework is:

$$\mathcal{L}_{total} = \mathcal{L}_{waypoint} + \mathcal{L}_{latent} + \mathcal{L}_{reward}, \quad (11)$$

where \mathcal{L}_{reward} is an optional loss depending on whether using the view selection approach. The weight of each loss is discussed in the implementation details.

5 Experiments

5.1 Setup

Open-loop Benchmark The open-loop benchmark uses recorded video streams of expert drivers along with the corresponding trajectories of the ego vehicle. We conduct our experiments on the nuScenes dataset [1], which comprises 1,000 driving scenes. In line with previous works [14, 16, 22], we employ Displacement Error (DE) and Collision Rate (CR) to comprehensively evaluate the

Table 1: **Comparison with State-of-the-art methods on the open-loop nuScenes [1] Benchmark.** FPS of ST-P3, VAD and LAW are tested on the NVIDIA Geforce RTX 3090 GPU. FPS of UniAD is tested on the NVIDIA Tesla A100 GPU. ‡ : LiDAR-based methods. We do not use any historical ego status information.

Method	L2 (m) ↓				Collision (%) ↓				Latency (ms)	FPS
	1s	2s	3s	Avg.	1s	2s	3s	Avg.		
NMP‡ [41]	-	-	2.31	-	-	-	1.92	-	-	-
SA-NMP‡ [41]	-	-	2.05	-	-	-	1.59	-	-	-
FF‡ [13]	0.55	1.20	2.54	1.43	0.06	0.17	1.07	0.43	-	-
EO‡ [23]	0.67	1.36	2.78	1.60	0.04	0.09	0.88	0.33	-	-
ST-P3 [14]	1.33	2.11	2.90	2.11	0.23	0.62	1.27	0.71	628.3	1.6
UniAD [15]	0.48	0.96	1.65	1.03	0.05	0.17	0.71	0.31	555.6	1.8
VAD [22]	0.41	0.70	1.05	0.72	0.07	0.17	0.41	0.22	224.3	4.5
LAW	0.26	0.57	1.01	0.61	0.14	0.21	0.54	0.30	51.2	19.5

planning performance. The Displacement Error measures the L2 distance between the predicted trajectory and the GT trajectory. The Collision Rate quantifies the rate of collisions that occur with other objects when following the predicted trajectory.

Closed-loop Benchmark Closed-loop evaluation is essential to autonomous driving as it constantly updates the sensor inputs based on the driving actions. The training dataset is collected from the CARLA [9] simulator (version 0.9.10.1) using the teacher model Roach [43] following [40, 20], resulting in 189K frames. We use the widely-used Town05 Long benchmark [20, 33, 11] to assess the closed-loop driving performance. We use the official metrics: Route Completion (RC) represents the percentage of the route completed by the autonomous agent. Infraction Score (IS) quantifies the number of infractions as well as violations of traffic rules. A higher Infraction Score indicates better adherence to safe driving practices. Driving Score (DS) is the primary metric used to evaluate overall performance. It is calculated as the product of Route Completion and Infraction Score.

Table 2: **Performance on closed-loop Town05 Long benchmark on CARLA.** Expert: Imitation learning from the driving trajectories of a privileged expert. Seg.: Semantic Segmentation. Map.: BEV Map Segmentation. Dep.: Depth Estimation. Det.: 3D Object Detection. *Latent Prediction*: our proposed self-supervised task.

Method	Supervision	DS↑	RC↑	IS↑
CILRS [7]	Expert	7.8±0.3	10.3±0.0	0.75±0.05
LBC [5]	Expert	12.3±2.0	31.9±2.2	0.66±0.02
Transfuser [30]	Expert, Dep., Seg., Map., Det.	31.0±3.6	47.5±5.3	0.77±0.04
Roach [43]	Expert	41.6±1.8	96.4±2.1	0.43±0.03
LAV [3]	Expert, Seg., Map., Det.	46.5±2.3	69.8±2.3	0.73±0.02
TCP [40]	Expert	57.2±1.5	80.4±1.5	0.73±0.02
MILE [11]	Expert, Map., Det.	61.1±3.2	97.4±0.8	0.63±0.03
ThinkTwice [21]	Expert, Dep., Seg., Det.	65.0±1.7	95.5±2.0	0.69±0.05
DriveAdapter [20]	Expert, Map., Det.	65.9±-	94.4±-	0.72±-
Interfuser [33]	Expert, Map., Det.	68.3±1.9	95.0±2.9	-
LAW	Expert, <i>Latent Prediction</i>	70.1±2.6	97.8±0.9	0.72±0.03

Implementation Details The default configuration of LAW does *not* include view selection unless specified. For the open-loop benchmark, we use Swin-Transformer-Tiny [26] (Swin-T) as the backbone. The input image is resized to 800 × 320. We employ a Cosine Annealing [27] learning rate schedule with an initial learning rate of 5e-5. AdamW [28] optimizer is utilized with a weight decay of 0.01 and we train the model with batch size 8 for 12 epochs on 8 RTX 3090 GPUs. The weight of the waypoint loss and latent prediction loss are set to 1.0. As for the planner with selected views, we finetune it with the reward loss based on the LAW. We set the initial learning rate to 5e-6 and train for an additional 6 epochs. The weight of the reward loss is set to 1.0. For the closed-loop benchmark. And we use ResNet-34 as the backbone following [40] for a fair comparison. We use

Table 3: **Ablation study on latent prediction.** The latent world model receives two types of inputs: view latents and predicted trajectory. No input refers to not utilizing the world model. Agg.: Aggregation. Pred.: Predicted. Traj.: Trajectory.

Temporal Agg.	Input of World Model		L2 (m) ↓				Collision (%) ↓			
	View Latent	Pred. Traj.	1s	2s	3s	Avg.	1s	2s	3s	Avg.
-	-	-	0.44	0.95	1.65	1.01	0.27	0.57	1.32	0.72
✓	-	-	0.32	0.67	1.14	0.71	0.20	0.30	0.73	0.41
✓	✓	-	0.30	0.64	1.12	0.68	0.18	0.27	0.66	0.37
✓	✓	✓	0.26	0.57	1.01	0.61	0.14	0.21	0.54	0.30

the TCP head [40] following [20]. The size of the input image is 900×256 . The optimizer is Adam. The learning rate is set to $1e-4$ and the weight decay is $1e-7$. We train the model with batch size 128 for 60 epochs. The learning rate is reduced by a factor of 2 after 30 epochs.

5.2 Comparison with State-of-the-art Methods

For the open-loop benchmark, we compare LAW with several state-of-the-art methods, including UniAD [15], VAD [22] on the nuScenes dataset. The results are summarized in Table 1. LAW outperforms UniAD and VAD in terms of the average L2 displacement error over 1s, 2s, and 3s prediction horizons. Moreover, our method achieves remarkable real-time performance with a latency of 30.9 ms, highlighting the efficiency of our approach. For the closed-loop benchmark, as shown in Table 2, our proposed method outperforms all existing methods. Notably, our approach surpasses previous leading methods such as ThinkTwice [21] and DriveAdapter [20], which incorporate extensive supervision from depth estimation, semantic segmentation, and map segmentation.

5.3 Ablation Study

Latent Prediction In this ablation study, we investigate the effectiveness of the latent prediction. The results are presented in Table 3. Initially, we only use the view latent as input of the world model, which means omitting the predicted trajectory component.

As shown in the third row of Table 3, this approach results in a slight performance improvement compared with the model without the latent prediction. When we include the predicted trajectory as part of the input (fourth row of Table 3), performance is significantly enhanced. It shows that an accurate prediction of future latents requires the incorporation of driving actions, highlighting the rationality of using the latent world model. Additionally, we provide an ablation study

on the latent prediction in the closed-loop setting, as depicted in Table 4. Notably, we observed substantial improvements in the Infraction Score. This indicates that the capability to predict future scenarios effectively aids in mitigating potential collisions.

Network Architecture of Latent World Model To validate the impact of the network architecture of the latent world model, we conduct experiments as shown in Table 5. Firstly, it is evident that a single-layer neural network, represented as Linear Projection, is not adequate for fulfilling the functions of the world model, resulting in significantly degraded performance. The two-layer MLP shows considerable improvement in performance. However, it lacks the capability to facilitate interactions among latents from different views. Therefore, we use the transformer decoder as our default network architecture, which achieves the best results among the tested architectures. This suggests that for any particular view, incorporating information from multiple adjacent views can enhance the prediction of its future latent.

The Time Horizon of Latent World Model In this experiment, the world model predicts latent features at three distinct future time horizons: 0.5 seconds, 1.5 seconds, and 3.0 seconds. This corresponds to the first, third, and sixth future frames from the current frame, given that keyframes

Table 4: **Ablation study on latent prediction on Town05 Long benchmark.**

Latent Prediction	DS↑	RC↑	IS↑
×	67.9±2.1	98.6±0.8	0.68±0.02
✓	70.1±2.6	97.8±0.9	0.72±0.03

Table 5: **Ablation study on different network architecture of the latent world model.** Linear Projection means a single-layer network. Arch.: Architecture.

World Model Arch.	L2 (m) ↓				Collision (%) ↓			
	1s	2s	3s	Avg.	1s	2s	3s	Avg.
Linear Projection	0.31	0.65	1.14	0.70	0.26	0.34	0.66	0.42
Two-layer MLP	0.27	0.58	1.07	0.64	0.17	0.23	0.59	0.33
Transformer Decoder	0.26	0.57	1.01	0.61	0.14	0.21	0.54	0.30

occur every 0.5 seconds in the nuScenes dataset. The results, displayed in Table 6, show that the model achieves the best performance at the 1.5-second horizon. The reasons are as follows. The 0.5-second interval typically presents scenes with minimal changes, providing insufficient dynamic content to improve feature learning. In contrast, the 3.0-second interval increases the complexity of the prediction task, which hinders better feature learning. This conclusion aligns with observations from MAE [10], where both excessively low and high mask ratios negatively impact the ability of the network.

Table 6: **Ablation study on the different time horizons for latent prediction.** The world model is capable of predicting latent at various future time horizons from the present moment.

Time Horizon	L2 (m) ↓				Collision (%) ↓			
	1s	2s	3s	Avg.	1s	2s	3s	Avg.
0.5s	0.26	0.57	1.01	0.61	0.14	0.21	0.54	0.30
1.5s	0.26	0.54	0.93	0.58	0.14	0.17	0.45	0.25
3.0s	0.28	0.59	1.01	0.63	0.13	0.20	0.48	0.27

View Selection To ablate the effectiveness of our view selection approach, we conduct the experiments shown in Table 7. We train our model with the view selection module and then test it with several strategies: 1) front view and a random view, 2) front view and a view selected by our view selection module, 3) front view and a view selected based on the rewards label in Sec. 4.3. This reward label is generated with the help of GT trajectory and this experiment serves as the upper bound. 4) all six views. The reason for fixing the front view will be discussed in the appendix A.1. The results demonstrate that the selection made by our view selection module significantly outperforms random selections and closely approaches the upper bound set by the GT.

Table 7: **Ablation study on the view selection approach.** We use the model trained with the selection reward prediction module for inference. GT view: We adopt the view selection strategy with the reward label instead of with the predicted reward.

Selected views	L2 (m) ↓				Collision (%) ↓				Latency (ms) ↓
	1s	2s	3s	Avg.	1s	2s	3s	Avg.	
Front + a random view	0.36	0.73	1.23	0.77	0.16	0.27	0.78	0.40	30.9
Front + predicted view	0.30	0.64	1.10	0.68	0.16	0.25	0.72	0.38	30.9
Front + GT view	0.28	0.56	0.97	0.60	0.15	0.22	0.61	0.33	30.9
Six views	0.26	0.57	1.01	0.61	0.14	0.21	0.54	0.30	51.2

6 Conclusion and Limitation

In conclusion, this paper introduces a novel self-supervised approach using the latent world model. This approach enhances the learning of scene representations in end-to-end autonomous driving systems without costly annotations. Although our method has demonstrated promising outcomes on current benchmarks, it is constrained by the limited volume of data utilized. In future work, we aim to enhance the scalability of our approach by applying it to larger and more diverse datasets. Leveraging large-scale data, we intend to employ the latent world model for pretraining.

References

- [1] Holger Caesar, Varun Bankiti, Alex H Lang, Sourabh Vora, Venice Erin Liong, Qiang Xu, Anush Krishnan, Yu Pan, Giancarlo Baldan, and Oscar Beijbom. nuscenes: A multimodal dataset for autonomous driving. In *CVPR*, 2020.
- [2] Sergio Casas, Abbas Sadat, and Raquel Urtasun. Mp3: A unified model to map, perceive, predict and plan. In *Proceedings of the IEEE/CVF Conference on Computer Vision and Pattern Recognition*, pages 14403–14412, 2021.
- [3] Dian Chen and Philipp Krähenbühl. Learning from all vehicles. In *Proceedings of the IEEE/CVF Conference on Computer Vision and Pattern Recognition*, pages 17222–17231, 2022.
- [4] Dian Chen, Brady Zhou, Vladlen Koltun, and Philipp Krähenbühl. Learning by cheating. In *Conference on Robot Learning*, pages 66–75. PMLR, 2020.
- [5] Dian Chen, Brady Zhou, Vladlen Koltun, and Philipp Krähenbühl. Learning by cheating. In *CoRL*, pages 66–75. PMLR, 2020.
- [6] Ting Chen, Simon Kornblith, Mohammad Norouzi, and Geoffrey Hinton. A simple framework for contrastive learning of visual representations. In *International conference on machine learning*, pages 1597–1607. PMLR, 2020.
- [7] Felipe Codevilla, Eder Santana, Antonio M López, and Adrien Gaidon. Exploring the limitations of behavior cloning for autonomous driving. In *ICCV*, 2019.
- [8] MMDetection3D Contributors. MMDetection3D: OpenMMLab Next-generation Platform for General 3D Object Detection. <https://github.com/open-mmlab/mmdetection3d>, 2020.
- [9] Alexey Dosovitskiy, German Ros, Felipe Codevilla, Antonio Lopez, and Vladlen Koltun. Carla: An open urban driving simulator. In *CoRL*, 2017.
- [10] Kaiming He, Xinlei Chen, Saining Xie, Yanghao Li, Piotr Dollár, and Ross Girshick. Masked autoencoders are scalable vision learners. In *CVPR*, pages 16000–16009, 2022.
- [11] Anthony Hu, Gianluca Corrado, Nicolas Griffiths, Zak Murez, Corina Gurau, Hudson Yeo, Alex Kendall, Roberto Cipolla, and Jamie Shotton. Model-based imitation learning for urban driving. *NeurIPS*, 2022.
- [12] Anthony Hu, Lloyd Russell, Hudson Yeo, Zak Murez, George Fedoseev, Alex Kendall, Jamie Shotton, and Gianluca Corrado. Gaia-1: A generative world model for autonomous driving. *arXiv preprint arXiv:2309.17080*, 2023.
- [13] Peiyun Hu, Aaron Huang, John Dolan, David Held, and Deva Ramanan. Safe local motion planning with self-supervised freespace forecasting. In *CVPR*, 2021.
- [14] Shengchao Hu, Li Chen, Penghao Wu, Hongyang Li, Junchi Yan, and Dacheng Tao. St-p3: End-to-end vision-based autonomous driving via spatial-temporal feature learning. In *ECCV*, 2022.
- [15] Yihan Hu, Jiazhi Yang, Li Chen, Keyu Li, Chonghao Sima, Xizhou Zhu, Siqi Chai, Senyao Du, Tianwei Lin, Wenhai Wang, et al. Goal-oriented autonomous driving. *arXiv preprint arXiv:2212.10156*, 2022.
- [16] Yihan Hu, Jiazhi Yang, Li Chen, Keyu Li, Chonghao Sima, Xizhou Zhu, Siqi Chai, Senyao Du, Tianwei Lin, Wenhai Wang, Lewei Lu, Xiaosong Jia, Qiang Liu, Jifeng Dai, Yu Qiao, and Hongyang Li. Planning-oriented autonomous driving. In *CVPR*, 2023.
- [17] Junjie Huang, Guan Huang, Zheng Zhu, and Dalong Du. Bevdet: High-performance multi-camera 3d object detection in bird-eye-view. *arXiv preprint arXiv:2112.11790*, 2021.
- [18] Yuanhui Huang, Wenzhao Zheng, Yunpeng Zhang, Jie Zhou, and Jiwen Lu. Tri-perspective view for vision-based 3d semantic occupancy prediction. In *Proceedings of the IEEE/CVF conference on computer vision and pattern recognition*, pages 9223–9232, 2023.
- [19] Bernhard Jaeger, Kashyap Chitta, and Andreas Geiger. Hidden biases of end-to-end driving models. In *ICCV*, 2023.
- [20] Xiaosong Jia, Yulu Gao, Li Chen, Junchi Yan, Patrick Langechuan Liu, and Hongyang Li. Driveadapter: Breaking the coupling barrier of perception and planning in end-to-end autonomous driving. In *ICCV*, 2023.

- [21] Xiaosong Jia, Penghao Wu, Li Chen, Jiangwei Xie, Conghui He, Junchi Yan, and Hongyang Li. Think twice before driving: towards scalable decoders for end-to-end autonomous driving. In *CVPR*, 2023.
- [22] Bo Jiang, Shaoyu Chen, Qing Xu, Bencheng Liao, Jiajie Chen, Helong Zhou, Qian Zhang, Wenyu Liu, Chang Huang, and Xinggang Wang. Vad: Vectorized scene representation for efficient autonomous driving. In *ICCV*, 2023.
- [23] Tarasha Khurana, Peiyun Hu, Achal Dave, Jason Ziglar, David Held, and Deva Ramanan. Differentiable raycasting for self-supervised occupancy forecasting. In *ECCV*, 2022.
- [24] Zhiqi Li, Wenhai Wang, Hongyang Li, Enze Xie, Chonghao Sima, Tong Lu, Qiao Yu, and Jifeng Dai. Bevformer: Learning bird’s-eye-view representation from multi-camera images via spatiotemporal transformers. *arXiv preprint arXiv:2203.17270*, 2022.
- [25] Yingfei Liu, Tiancai Wang, Xiangyu Zhang, and Jian Sun. Petr: Position embedding transformation for multi-view 3d object detection. In *European Conference on Computer Vision*, pages 531–548. Springer, 2022.
- [26] Ze Liu, Yutong Lin, Yue Cao, Han Hu, Yixuan Wei, Zheng Zhang, Stephen Lin, and Baining Guo. Swin transformer: Hierarchical vision transformer using shifted windows. In *Proceedings of the IEEE/CVF International Conference on Computer Vision (ICCV)*, 2021.
- [27] Ilya Loshchilov and Frank Hutter. Sgdr: Stochastic gradient descent with warm restarts. *arXiv preprint arXiv:1608.03983*, 2016.
- [28] Ilya Loshchilov and Frank Hutter. Decoupled weight decay regularization. *arXiv preprint arXiv:1711.05101*, 2017.
- [29] Chen Min, Dawei Zhao, Liang Xiao, Jian Zhao, Xinli Xu, Zheng Zhu, Lei Jin, Jianshu Li, Yulan Guo, Junliang Xing, et al. Driveworld: 4d pre-trained scene understanding via world models for autonomous driving. *arXiv preprint arXiv:2405.04390*, 2024.
- [30] Aditya Prakash, Kashyap Chitta, and Andreas Geiger. Multi-modal fusion transformer for end-to-end autonomous driving. In *CVPR*, 2021.
- [31] Katrin Renz, Kashyap Chitta, Otniel-Bogdan Mercea, A Koepke, Zeynep Akata, and Andreas Geiger. Plant: Explainable planning transformers via object-level representations. *arXiv preprint arXiv:2210.14222*, 2022.
- [32] Abbas Sadat, Sergio Casas, Mengye Ren, Xinyu Wu, Pranaab Dhawan, and Raquel Urtasun. Perceive, predict, and plan: Safe motion planning through interpretable semantic representations. In *ECCV*, 2020.
- [33] Hao Shao, Letian Wang, RuoBing Chen, Hongsheng Li, and Yu Liu. Safety-enhanced autonomous driving using interpretable sensor fusion transformer. *CoRL*, 2022.
- [34] Hao Shao, Letian Wang, Ruobing Chen, Steven L Waslander, Hongsheng Li, and Yu Liu. ReasonNet: End-to-End Driving with Temporal and Global Reasoning. In *CVPR*, pages 13723–13733, 2023.
- [35] Marin Toromanoff, Emilie Wirbel, and Fabien Moutarde. End-to-end model-free reinforcement learning for urban driving using implicit affordances. In *CVPR*, 2020.
- [36] Aaron Van Den Oord, Oriol Vinyals, et al. Neural discrete representation learning. *Advances in neural information processing systems*, 30, 2017.
- [37] Qitai Wang, Yuntao Chen, Ziqi Pang, Naiyan Wang, and Zhaoxiang Zhang. Immortal tracker: Tracklet never dies. *arXiv preprint arXiv:2111.13672*, 2021.
- [38] Yuqi Wang, Yuntao Chen, Xingyu Liao, Lue Fan, and Zhaoxiang Zhang. Panoocc: Unified occupancy representation for camera-based 3d panoptic segmentation. *arXiv preprint arXiv:2306.10013*, 2023.
- [39] Yuqi Wang, Jiawei He, Lue Fan, Hongxin Li, Yuntao Chen, and Zhaoxiang Zhang. Driving into the future: Multiview visual forecasting and planning with world model for autonomous driving. *arXiv preprint arXiv:2311.17918*, 2023.
- [40] Penghao Wu, Xiaosong Jia, Li Chen, Junchi Yan, Hongyang Li, and Yu Qiao. Trajectory-guided control prediction for end-to-end autonomous driving: a simple yet strong baseline. *NeurIPS*, 2022.
- [41] Wenyuan Zeng, Wenjie Luo, Simon Suo, Abbas Sadat, Bin Yang, Sergio Casas, and Raquel Urtasun. End-to-end interpretable neural motion planner. In *CVPR*, 2019.

- [42] Lunjun Zhang, Yuwen Xiong, Ze Yang, Sergio Casas, Rui Hu, and Raquel Urtasun. Learning unsupervised world models for autonomous driving via discrete diffusion. *arXiv preprint arXiv:2311.01017*, 2023.
- [43] Zhejun Zhang, Alexander Liniger, Dengxin Dai, Fisher Yu, and Luc Van Gool. End-to-end urban driving by imitating a reinforcement learning coach. In *ICCV*, 2021.
- [44] Wenzhao Zheng, Weiliang Chen, Yuanhui Huang, Borui Zhang, Yueqi Duan, and Jiwen Lu. Occworld: Learning a 3d occupancy world model for autonomous driving. *arXiv preprint arXiv:2311.16038*, 2023.
- [45] Xingyi Zhou, Vladlen Koltun, and Philipp Krähenbühl. Tracking objects as points. In *European conference on computer vision*, pages 474–490. Springer, 2020.

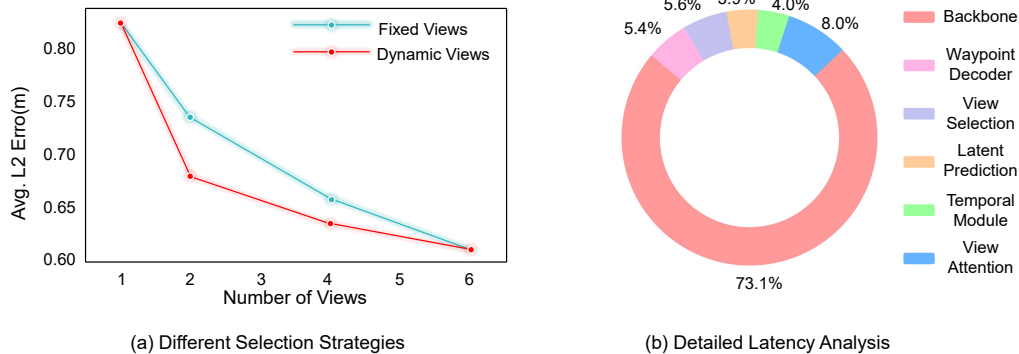


Figure 4: (a) Comparison between different selection strategies. (b) Detailed latency analysis.

A Appendix

A.1 More Analysis of View Selection

In our view selection approach, we always use the front view and dynamically choose one additional view from the other five views. The reason for doing this is driven by the following experiments.

Fixing Front View Helps This section presents the experimental justification for always choosing the front camera view as one of the input views. Specifically, given the trained end-to-end planner without reward loss, we conduct two view-selection strategies on it. The first strategy always uses the front camera and selects one random view from the remaining five cameras. The second strategy randomly chooses two cameras. The results are shown in Table 8. This experiment shows that the strategy of fixing the front view and randomly selecting an additional view outperforms the random selection of two views. This superiority can be attributed to the fact that the front view can provide more crucial information for the planning task, especially in forward-driving scenarios.

Table 8: The importance of front view.

Selected Views	L2 (m) ↓				Collision (%) ↓			
	1s	2s	3s	Avg.	1s	2s	3s	Avg.
Two random views	0.39	0.79	1.32	0.83	0.15	0.28	0.91	0.45
Front + a random view	0.36	0.74	1.24	0.78	0.16	0.28	0.82	0.42

Different Selection Strategy Reducing the number of *fixed cameras* can also alleviate the computational burden. Therefore, it is natural to question how the view selection approach compares to a configuration utilizing a reduced number of fixed cameras. To investigate this, we carry out experiments as illustrated in Fig. 4 (a). The specific settings of the experiments are as follows. We set up four groups of experiments with the number of views used being 1, 2, 4, and 6. When using only one view, we always use the front camera. For two views, the fixed-view model is trained and tested using the front and back cameras, while the dynamic-view model (i.e., our method) fixes the front camera and then selects the most informative view from the remaining five cameras. For four views, the fixed-view model uses the front, front-left, front-right, and back cameras, while the dynamic-view model fixes the front camera and chooses three additional cameras from the remaining five. Finally, for six views, we use all available cameras. The results demonstrate that our dynamic selection method consistently outperforms fixed-view settings with the same number of views. This indicates that our method is capable of selecting the informative views from multiple options.

Latency Breakdown Our Planner with Selected Views attains an impressive speed of 32.4 FPS. Here we present the detailed latency of each module. We test it on the NVIDIA Geforce RTX 3090 GPU with batch size 1. The code is based on the mmdetection3d [8]. The specific latency associated with each module in our model is detailed in Fig. 4 (b). As illustrated in the figure, the backbone constitutes the majority of the model’s latency. Reducing the number of input views leads to a linear

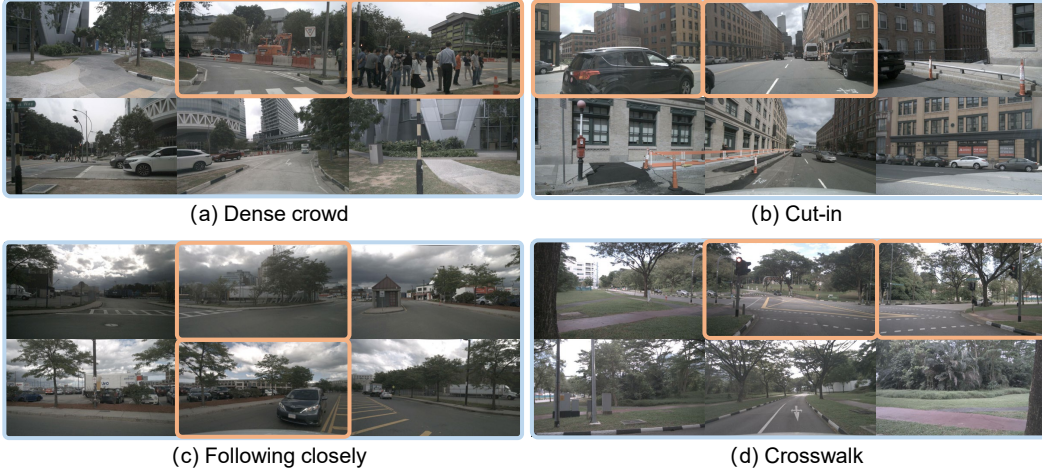


Figure 5: **The visualization of view selection.** We outline the selected views in orange boxes.

decrease in the cost of the backbone. Since we only have two views passing through the backbone, our view-selection method substantially boosts the efficiency.

View Selection Visualization As depicted in Fig. 5, we present a visualization analysis of four typical cases. From these visualizations, we derive two key insights: 1) Our method has a preference for views with visually salient objects. As demonstrated in cases (a), (b), and (c), the model tends to select views that feature groups of people, vehicles with the potential to cut in, or vehicles at risk of a rear-end collision. This preference arises because such objects have a significant impact on driving behavior. Through reward learning, our model can identify the view that is most important at a certain moment, by the clues offered by these salient objects. 2) Our model learns prior knowledge of specific scenarios. Human drivers have prior knowledge about the world, such as the expectation of pedestrians suddenly appearing at crosswalks, which necessitates slower driving. Our view latent reconstruction module can also learn similar priors. For instance, in case (d), the view selection model, aided by the reconstruction module, reasonably focuses on the crosswalk.